1 **Revision 1 (Manuscript 9060)**

2 **Word Count: 5327**

3 # Different structural behavior of $MgSiO_3$ and $CaSiO_3$ glasses at high pressures

4 Nozomi M. Kondo[1, 2*], Yoshio Kono[1], Itaru Ohira[3], Rostislav Hrubiak[4], Koji Ohara[5],

5 Kiyofumi Nitta[5], Oki Sekizawa[5]

6 [1]Geodynamics Research Center, Ehime University, 2-5 Bunkyo-cho, Matsuyama, Ehime

7 790-0826, Japan

8 [2]Now at Institute for Planetary Materials, Okayama University, 827 Yamada, Misasa,

9 Tottori 682-0193, Japan

10 [3]Department of Chemistry, Gakushuin University, Mejiro, Toshima-ku, Tokyo 171-8588,

11 Japan

12 [4]High Pressure Collaborative Access Team, X-ray Science Division, Argonne National

13 Laboratory, 9700 S.Cass Avenue, Argonne, IL 60439, United States

14 [5]SPring-8 synchrotron facility, Japan Synchrotron Radiation Research Institute, 1-1-1

15 Kouto, Sayo-cho, Sayo-gun, Hyogo 679-5198, Japan

* Corresponding author: nozomikondo@okayama-u.ac.jp (N. M. Kondo)

Abstract

Knowledge of the structural behavior of silicate melts and/or glasses at high pressures provides fundamental information in discussing the nature and properties of silicate magmas in the Earth's interior. The behavior of Si-O structure under high pressure conditions has been widely studied, while the effect of cation atoms on the high-pressure structural behavior of silicate melts or glasses has not been well investigated. In this study, we investigated the structures of $MgSiO_3$ and $CaSiO_3$ glasses up to 5.4 GPa by in-situ X-ray pair distribution function measurements, to understand the effect of different cations (Mg^{2+} and Ca^{2+}) on high pressure structural behavior of silicate glasses. We found that the structural behavior of $MgSiO_3$ and $CaSiO_3$ glasses are different at high pressures. The structure of $MgSiO_3$ glass changes by shrinking of Si-O-Si angle with increasing pressures, which is consistent with previous studies for SiO_2 and $MgSiO_3$ glasses. On the other hand, $CaSiO_3$ glass shows almost no change in Si-Si distance at high pressures, while the intensities of two peaks at ~3.0 Å and ~3.5 Å change with increasing pressure. The structural change in $CaSiO_3$ glass at high pressure is interpreted as the change of the

fraction of the edge-shared and corner-shared CaO_6-SiO_4 structures. The different high-pressure structural behavior obtained in $MgSiO_3$ and $CaSiO_3$ glasses may be structural origin of the difference in the properties such as viscosity between $MgSiO_3$ and $CaSiO_3$ melts at high pressures, implying the importance of the different structural behavior due to different cation atoms to discuss the nature and properties of silicate magmas in the Earth's interior.

Keywords: glass structure, $MgSiO_3$, $CaSiO_3$, pair distribution function, high pressure

Introduction

Structures of silicate melts strongly influence physical properties such as density, viscosity, and diffusivity (e.g., Sakamaki et al., 2013; Sanloup et al., 2013; Wang et al., 2014; Bajgain et al., 2015), and therefore knowledge of the structural behavior of silicate melts and/or glasses under high pressure conditions is fundamental in understanding the nature and properties of silicate magmas in the Earth's interior. Since structural investigation of silicate melts under in situ high pressure and high temperature condition is

still challenging, due to the technical difficulties, silicate glasses have been studied at high pressures under room temperature condition as an analogue of silicate melts. Pressure-induced structural changes of SiO_2 glass have been the most studied as the simplest silicate composition by using in situ high-pressure techniques (e.g., Sato and Funamori, 2008; Benmore et al., 2010; Murakami and Bass, 2010; Prescher et al., 2017; Lee et al., 2019; Petitgirard et al., 2019; Kono et al., 2020; Andrault et al., 2020, Kono et al., 2022), which provide important knowledge on the behavior of Si-O structure under high pressure conditions. In addition, $MgSiO_3$ glass also has been studied by several researchers as a representative composition of silicate magma in the Earth's interior (e.g., Lee et al., 2008; Kono et al., 2018; Salmon et al., 2019; Ryu et al., 2022). However, structural behavior of other silicate glasses with different compositions remains not well investigated at in situ high-pressure conditions.

In this study, we investigate structure of $MgSiO_3$ and $CaSiO_3$ glasses at high pressure conditions up to 5.4 GPa by using in situ pair distribution function measurements, to understand the effect of different cations (Mg^{2+} and Ca^{2+}) on the high-pressure structural behavior of silicate glasses. $MgSiO_3$ and $CaSiO_3$ glasses are the end-member pyroxene compositions, and therefore knowledge of the structural behavior of $MgSiO_3$ and $CaSiO_3$

glasses at high pressures would provide important clues to understand structure and properties of silicate magmas in the Earth's upper mantle. At ambient pressure condition, structures of $MgSiO_3$ and $CaSiO_3$ glasses have been studied by neutron diffraction (e.g., Cormier and Cuello, 2011), high energy X-ray diffraction (Kohara et al., 2011), Raman spectroscopy (e.g., Kalampounias et al., 2009), and nuclear magnetic resonance (NMR) spectroscopy (e.g., Kaseman et al., 2015) techniques. On the other hand, structural investigations of these glasses at in situ high pressure conditions are still limited, although there are several structural analyses for the high-pressure synthesized silicate glasses at ambient pressure condition (Shimoda et al., 2005). Nevertheless, structure of $MgSiO_3$ glass at in situ high pressure conditions has been studied by some previous studies using neutron diffraction (Salmon et al., 2019), X-ray diffraction (Kono et al., 2018; Ryu et al., 2022), and X-ray Raman scattering (Lee et al., 2008) measurements. In contrast, structure of $CaSiO_3$ glass has not been well studied at in situ high pressure conditions. To the best of our knowledge, only Kubicki et al. (1992) and Salmon et al. (2019) investigated the structure of $CaSiO_3$ glass at in situ high pressure conditions. Kubicki et al. (1992) conducted in-situ Raman spectroscopy and infrared absorption measurements on $CaSiO_3$ glasses in DAC (diamond anvil cell) at 11-35 GPa. Salmon et al. (2019) investigated the structure of

82 $CaSiO_3$ and $MgSiO_3$ glasses from ambient pressure to 17.5 GPa by using in-situ neutron
83 diffraction measurement and molecular dynamics (MD) simulation. Salmon et al. (2019)
84 showed that the M-O (M=Mg, Ca) coordination number of both $CaSiO_3$ and $MgSiO_3$
85 glasses increase at high pressures in a similar manner. The nearest neighbor Si-O and M-O
86 distances show slight increase with increasing pressure from ambient pressure to 17.5 GPa
87 (1.61 to 1.62Å for Si-O distance of $MgSiO_3$ glass; 1.62 to 1.63 Å for Si-O distance of
88 $CaSiO_3$ glass; 1.99-2.02 Å for Mg-O distance in $MgSiO_3$ glass; 2.32-2.35 Å for Ca-O
89 distance in $CaSiO_3$ glass). Mg-O coordination number in $MgSiO_3$ glass changes from 4.50
90 at ambient pressure to 6.20 at 17.5 GPa, and Ca-O coordination number in $CaSiO_3$ glass
91 changes from 6.15 at ambient pressure to 7.41 at 17.5 GPa. These data indicate that the
92 nearest neighbor structures in $MgSiO_3$ and $CaSiO_3$ glasses change similarly with increasing
93 pressure. However, the study of Salmon et al. (2019) was limited only for the nearest
94 neighbor Si-O and M-O distances, due to weak scattering of Si and Ca in neutron
95 diffraction measurement, and the intermediate range structure such as Si-Si, Ca-Si and Ca-
96 Ca distances have not been investigated in Salmon et al. (2019).

97 In this study, we investigated structures of $MgSiO_3$ and $CaSiO_3$ glasses at high
98 pressures up to 5.4 GPa by using in-situ X-ray diffraction measurements to understand

effect of different cation (Mg and Ca) on the high-pressure structural behavior not only in the nearest Si-O and M-O distances but also in the intermediate Si-Si, M-Si, and M-M distances. We found different behavior in the intermediate range structures of $MgSiO_3$ and $CaSiO_3$ glasses at high pressure conditions.

Experimental methods

$CaSiO_3$ and $MgSiO_3$ samples were prepared by mixing powders of SiO_2, $CaCO_3$, and/or MgO. Powders of these oxides and carbonates were dried at 110 °C for >24 hours before weighing with an electric balance, and were mixed in an agate mortar with ethanol for 1-2 hours. Glass samples were prepared by an aerodynamic levitation furnace with CO_2 laser heating at ~1800-2100 °C at Geodynamics Research Center (GRC), Ehime University. Chemical compositions of the synthesized glass samples were confirmed by using JEOL JM-7000F field-emission scanning electron microscope (FE-SEM) with energy-dispersive spectroscopy (EDS) at GRC (Table S1). Densities of the $CaSiO_3$ (2.80±0.05 g/cm^3) and $MgSiO_3$ (2.68±0.06 g/cm^3) glasses were measured by Archimedes' method.

High-energy X-ray diffraction measurements of the $CaSiO_3$ and $MgSiO_3$ glasses at

115 ambient pressure were conducted at the BL04B2 beamline of the SPring-8. The dedicated
116 X-ray diffractometer with six points detectors (four cadmium telluride detectors and two
117 germanium detectors) at the BL04B2 beamline enables us to conduct accurate pair
118 distribution function (PDF) analysis with high-real space resolution (Ohara et al, 2020). We
119 used spherical glass samples of 1.8 mm diameter, which were placed in a vacuum chamber
120 under room temperature condition. High-energy X-ray diffraction measurements using
121 monochromatic X-ray of 61.4 keV were carried out by scanning the 2θ angle from 0.3 to 49
122 degrees, which covers the range of the momentum transfer Q up to 25.5 $Å^{-1}$. The obtained
123 X-ray diffraction data were analyzed by using standard analysis procedures of the BL04B2
124 beamline (Kohara et al., 2007).

125 High-pressure experiments for $CaSiO_3$ and $MgSiO_3$ glasses were carried out by using
126 a Paris-Edinburgh (PE) press with a standard PE cell assembly of the 16-BM-B beamline in
127 the Advanced Photon Source (APS) (Kono et al., 2014). Cup-shaped WC anvils with the
128 cup diameter of 12 mm and the bottom diameter of 3 mm were used. The cell assembly
129 mainly consists of BN capsule surrounded by inner MgO ring and outer boron-epoxy (BE)
130 gaskets with ZrO_2 caps at the top and bottom the cell. Pressure was determined by X-ray
131 diffraction measurement of MgO ring with the equation of state of MgO (Kono et al., 2010)

for the $CaSiO_3$ glass experiment, and of Au foil, which is inserted between the MgO ring and BN capsule, using the equation of state of Tsuchiya (2003) for the $MgSiO_3$ glass experiment. Densities of $CaSiO_3$ and $MgSiO_3$ glasses at high pressure conditions are calculated based on the densities of $CaSiO_3$ (2.80±0.05 g/cm^3) and $MgSiO_3$ (2.68±0.06 g/cm^3) glasses measured at ambient pressure by Archimedes' method and the pressure-volume relation of $CaSiO_3$ and $MgSiO_3$ glasses reported in Salmon et al. (2019).

Pair distribution function measurement of $CaSiO_3$ glass at high pressures was carried out by a multi-angle energy dispersive X-ray diffraction technique combined with the PE cell at the 16-BM-B beamline of the APS. A large Huber stage holding a germanium solid state detector allows precise control of 2θ angles, and energy dispersive X-ray diffraction measurements using fine collimation slits enables us to collect clean signals from glass sample without background noise from the surrounding pressure medium materials (Kono et al., 2014). We collected energy dispersive X-ray diffraction patterns at the 2θ angles of 3, 4, 5, 7, 9, 12, 16, 22, 28, and 35 degrees. The obtained energy dispersive X-ray diffraction spectra were analyzed by using an analysis program developed by Changyong Park and Rostislav Hrubiak at the 16-BM-B beamline (Kono et al., 2014). We obtained the $S(Q)$ of $CaSiO_3$ glass at the Q range up to 17.0 Å^{-1} under the pressure conditions from 0.8 GPa to

149 5.4 GPa at room temperature.

150 Pair distribution function measurement of $MgSiO_3$ glass at high pressures was
151 conducted at the BL37XU beamline of the SPring-8. We used a monochromatic X-ray of
152 37.4 keV. The X-ray was focused from 1.0 to 0.2 mm in horizontal with 0.7-m-long
153 horizontal-deflection mirrors so as to increase an available flux. The structure of $MgSiO_3$
154 glass was measured up to 5.2 GPa in the PE cell by high-energy X-ray diffraction
155 measurement using a cadmium telluride point detector (Amptek X-123) with a double slit
156 collimation setup in front of the detector. The double slit collimation setup yields
157 collimation length of <1.8 mm at the sample position at 2θ angles higher than ~9˚, to avoid
158 background noises. Size of incident slit and two collimation slits were adjusted with
159 varying 2θ angle to maximize intensity of signal by increasing collimation length within the
160 diameter of $MgSiO_3$ glass sample. High-energy X-ray diffraction measurements for
161 $MgSiO_3$ glass at high pressures were carried out by scanning the 2θ angle from 1 to 60
162 degrees. Analysis was conducted by using the method developed at the BL04B2 beamline
163 of the SPring-8 (Ohara et al., 2020). We obtained the $S(Q)$ of $MgSiO_3$ glass at the Q range
164 up to 15.0 $Å^{-1}$ under the pressure conditions from 1.0 GPa to 5.2 GPa at room temperature.

165 It is important to note that both experiments at BL37XU beamline at SPring-8

166 ($MgSiO_3$ glass experiment) and at 16-BM-B beamline at APS ($CaSiO_3$ glass experiment)
167 used collimation slit setup in front of the detector. The collimation slit setup enables us to
168 collect the XRD signal only from the sample at the 2θ angle higher than ~9° for the
169 $MgSiO_3$ glass experiment and at the 2θ angle higher than ~3° for the $CaSiO_3$ glass
170 experiment. Since the collimation slit setup eliminates back-ground noises not only from
171 the high-pressure cell assemblies but also from different beamline component, we can
172 obtain comparable data.

173 The pair distribution function $g(r)$ was obtained by Fourier transmission of the Faber-
174 Ziman total structure factor $S(Q)$ (Faber and Ziman, 1965). The Lorch function was applied
175 to remove the truncation effect on the final pair distribution function determination (Lorch,
176 1969). The positions of the peaks of the *g(r)* showing discernible separation were
177 determined by using simple Gaussian peak fitting. On the other hand, Si-Si, Mg-Si, and
178 Mg-Mg peaks in $MgSiO_3$ glass, and Ca-O and O-O peaks in $CaSiO_3$ glass overlap each
179 other. For the overlapping peaks, we used a multi-peak fitting method described in de
180 Grouchy et al. (2017). In the de Grouchy et al.'s method, the *g(r)* is the sum of all the
181 individual ion-ion interactions within the sample, where each ion-ion contribution is
182 represented by a Gaussian peak, $g(r)_{ind}$. The *g(r)* is fit using the following equations:

This is the peer-reviewed, final accepted version for American Mineralogist, published by the Mineralogical Society of America.
The published version is subject to change. Cite as Authors (Year) Title. American Mineralogist, in press.
DOI: https://doi.org/10.2138/am-2023-9060. http://www.minsocam.org/

$$g(r) = \sum g(r)_{ind} = \frac{1}{n_0 S} \sum_i \frac{x_i A_i}{\sigma_{i\sqrt{2\pi}}} \exp\left(\frac{-(r-d_i)^2}{2\sigma_i^2}\right), \qquad (1)$$

where

$$A_i = \frac{CN_i}{\int \frac{4\pi r^2}{\sigma_i\sqrt{2\pi}} exp - \left(\frac{(r-d_i)^2}{2\sigma_i^2}\right) dr}, \qquad (2)$$

where CN_i is coordination number for individual ion-ion contributions, n_0 is number density, x_i is concentration of the species, and d_i is interatomic distance. σ_i is calculated from $k\sqrt{d_i}$, which defines width and height of the individual Gaussian peak. k is an adjustable parameter (Hosemann and Bagchi, 1962), with values ranging from 0.06 to 0.15 depending on the ion-ion contribution.

Results

Structure of $MgSiO_3$ and $CaSiO_3$ glasses at ambient pressure

Figures 1a and 1b show the $S(Q)$ and $g(r)$ of $MgSiO_3$ glass at ambient pressure, respectively. The $g(r)$ of $MgSiO_3$ glass shows peaks at r_1=1.621±0.002 Å, r_2=2.030±0.004 Å, r_3=2.618±0.009 Å, and r_4=3.179±0.006 Å. A first-principles molecular dynamics simulation of $MgSiO_3$ glass reports bond distances of Si-O=1.63 Å, Mg-O=1.98 Å, O-O=2.68 Å, Si-Si=3.02 Å, Mg-Si=3.22 Å, and Mg-Mg=3.42 Å (Ghosh et al., 2014), indicating that the r_1, r_2, and r_3 peaks obtained in this study correspond to Si-O, Mg-O, and

198 O-O distances, respectively. The r_4 peak is considered as overlapping of Si-Si, Mg-Si, and
199 Mg-Mg distances.

200 The $S(Q)$ and $g(r)$ of $CaSiO_3$ glass at ambient pressure are shown in Figs. 1c and 1d,
201 respectively. The *g(r)* of $CaSiO_3$ glass shows the peak positions at r_1=1.622±0.001 Å,
202 r_2=2.335±0.008 Å, r_3=2.623±0.012 Å, r_4=3.017±0.008 Å, and r_5=3.573±0.014 Å, which are
203 considered as Si-O, Ca-O, O-O, Si-Si/Ca-Si, and Ca-Si/Ca-Ca distances, respectively
204 (Cormier and Cuello, 2013; Mead and Mountjoy, 2006ab). According to a molecular
205 dynamics simulation study (Mead and Mountjoy, 2006ab), Si-Si and Ca-Si distances
206 overlap at the same distance at around 3.1 Å, and Ca-Si and Ca-Ca distances also overlap at
207 around 3.6 Å.

208

209 **Structures of $MgSiO_3$ and $CaSiO_3$ glasses at high pressures**

210 Figures 2a and 2b show the $S(Q)$ and $g(r)$ of $MgSiO_3$ glass from 1.0 to 5.2 GPa.
211 With increasing pressure, intensity of the first sharp diffraction peak (FSDP) of $MgSiO_3$
212 glass decreases, and the FSDP position shifts toward high Q (Figs. 2a and 3). The high-
213 pressure behaviour of the FSDP is consistent with those reported in previous $MgSiO_3$ glass
214 study (e.g., Ryu et al., 2022). On the other hand, the *S(Q)* of $MgSiO_3$ glass shows negligible

change at Q>3 Å^{-1} at high pressure conditions up to 5.2 GPa. The $g(r)$ of $MgSiO_3$ glass shows clear r_1 (Si-O) and r_4 (Si-Si/Mg-Si/Mg-Mg) peaks (Fig. 2b). On the other hand, the r_2 (Mg-O) peak is identified as a shoulder peak on the high r side of the r_1 (Si-O) peak, and the r_3 (O-O) peak is not visible. This is due to broadening of the peak width of $g(r)$ by narrower range of Q (15 Å^{-1}) in the $S(Q)$ data obtained in the high pressure experiments. Fig. S1 shows the effect of the maximum Q (Q_{max}) range on the $g(r)$ simulated by using the ambient pressure data. The resolution of the $g(r)$ is defined as $2\pi/Q_{max}$ (e.g., Lorch, 1969), and the peak width of $g(r)$ becomes broader by reducing the Q_{max}. In Fig. S1a, the $g(r)$ result simulated with the Q_{max}=15 Å^{-1} shows the r_2 peak as the shoulder peak of the r_1 peak, similarly to the high-pressure experimental result, and it is difficult to identify the r_3 peak. On the other hand, the peak positions of $g(r)$ determined from the result of Q_{max}=15 Å^{-1} (r_1=1.619±0.003 Å; r_2=2.029±0.010 Å; r_4=3.183±0.003 Å; r_3 is fixed at 2.618 Å) are comparable to those obtained from the data of Q_{max}=25 Å^{-1} (r_1=1.621±0.002 Å; r_2=2.030±0.004 Å; r_3=2.618±0.003 Å; r_4=3.179±0.003 Å). Therefore, the peak positions of the $g(r)$ of $MgSiO_3$ glass at high pressures determined from the $S(Q)$ of Q_{max}=15 Å^{-1} are considered to be comparable to those determined at ambient pressure. The $g(r)$ of $MgSiO_3$ glass at high pressures shows almost no change in the r_1 and r_2 peaks up to 5.2 GPa, while

the position of the r_4 peak decreases with increasing pressure (Fig. 2b).

Figures 2c and 2d show the $S(Q)$ and $g(r)$ of $CaSiO_3$ glass from 0.8 to 5.4 GPa. In contrast to the marked change in the FSDP of $MgSiO_3$ glass at high pressures, the $S(Q)$ of $CaSiO_3$ glass shows only small change in the intensity and position of the FSDP at high pressures (Figs. 2c and 3). On the other hand, the second and third peak features in the $S(Q)$ at around 4-6 $Å^{-1}$ shift toward high Q with increasing pressure (Fig. 2c). The *g(r)* of $CaSiO_3$ glass obtained at high pressures show clear r_1 (Si-O), r_2 (Ca-O), r_4 (Si-Si/Ca-Si), and r_5 (Ca-Si/Ca-Ca) peaks (Fig. 2d). The Ca-O peak of the $g(r)$ in $CaSiO_3$ glass can be well identified even at the narrower range of Q_{max} (17 $Å^{-1}$) in the $S(Q)$ of the high-pressure experiments (Fig. S1a), because of longer distance of Ca-O peak in $CaSiO_3$ glass compared to Mg-O peak in $MgSiO_3$ glass. In addition, comparison of the peak positions of $CaSiO_3$ glass at ambient pressure determined by the Q range of 17 $Å^{-1}$ (r_1=1.614±0.003 Å; r_2=2.358±0.008 Å; r_4=3.077±0.165 Å; r_5=3.560±0.021 Å) and 25 $Å^{-1}$ (r_1=1.622±0.001 Å; r_2=2.335±0.008 Å; r_4=3.017±0.008 Å; r_5=3.573±0.014 Å) show similar values. The r_1 and r_2 peaks of the $g(r)$ of $CaSiO_3$ glass stay almost same up to 5.4 GPa, while there are marked changes in the intensity of the r_4 and r_5 peaks with increasing pressure (Fig. 2d). The intensity of the r_4 peak markedly increases with increasing pressure, accompanied with the decrease of the

intensity of the r_5 peak. The position of the r_4 peak stays almost same up to 5.4 GPa, while the position of the r_5 peak slightly decreases with increasing pressure.

Table 1 summarizes the positions of the FSDP of $S(Q)$, the $g(r)$ peak positions, Si-O-Si angle of $MgSiO_3$ glass, and Si-O-Si/Ca-O-Si angles of $CaSiO_3$ glass from ambient to high pressures. Since the r_3 and r_4 peaks of $MgSiO_3$ glass are overlapped by O-O, Si-Si, Mg-Si, and Mg-Mg distances, we carried out multi-peak fitting procedure with the method of de Grouchy et al. (2017). We firstly fitted O-O, Si-Si, Mg-Si, and Mg-Mg peaks into the r_3 and r_4 peaks at ambient pressure (using the Q_{max}=15 $Å^{-1}$ data) by referring the bond distances and the coordination numbers reported in Ghosh et al. (2014). The *g(r)* at ambient pressure is well reproduced by the parameters of Ghosh et al. (2014) with minor adjustment for O-O and Si-Si distances (Fig. S2a). Then, the Si-Si and Mg-Si peak positions at high pressures were determined by fixing widths and heights of all peaks, and peak positions of O-O and Mg-Mg (2.65 and 3.42 Å, respectively) (Fig. S2). It has been reported in SiO_2 glass that O-O distance does not change at least up to 6.0 GPa, because of almost no change of Si-O tetrahedron structure (Kono et al., 2022). Since our observed Si-O distances of $MgSiO_3$ and $CaSiO_3$ glasses also do not change with varying pressure (cf. Fig. 4), we assumed no change in O-O peak distance in $MgSiO_3$ glass at the pressure range of this

study up to 5.4 GPa. For Mg-Mg distance of $MgSiO_3$ glass, MD simulations of Salmon et al. (2019) show that Mg-O bond distance and Mg-O-Mg angle do not change below 6 GPa, which indicates no change in Mg-Mg distance. We therefore assumed that the Mg-Mg distance have no pressure dependence at the pressure range of this study ($\leq$ 5.2 GPa).

In addition, the Ca-O distances of $CaSiO_3$ glass at high pressure conditions are determined also by the peak-fitting method of de Grouchy et al. (2017), because the r_3 (O-O) peak of the *g(r)* of $CaSiO_3$ glass is hidden around the right side shoulder of the r_2 (Ca-O) peak in the high-pressure data. Firstly, we fitted r_2 (Ca-O) and r_3 (O-O) peak positions at ambient pressure (using the Q_{max}=25 $Å^{-1}$ data) by fixing the coordination numbers reported in Mead and Mountjoy (2006b) and Bajgain et al. (2015). Our obtained Ca-O [2.302(±0.001) Å] and O-O [2.611(±0.007) Å] distances at ambient pressure condition are consistent with those reported in Mead and Mountjoy (2006b) and Bajgain et al. (2015). Then, we fitted r_2 (Ca-O) peak positions of $CaSiO_3$ glass at high pressures by fixing coordination number and O-O peak position obtained at ambient pressure (Figure S3).

Discussion

Figure 4 shows the nearest-neighbor Si-O and M-O (M=Mg, Ca) distances (Fig.4a)

283 and the intermediate range Si-Si and M-Si distances (Fig. 4b) of $MgSiO_3$ and $CaSiO_3$
284 glasses at high pressures. The Si-O peak positions of $MgSiO_3$ and $CaSiO_3$ glasses are same,
285 while the positions of the M-O peaks are markedly different between $MgSiO_3$ and $CaSiO_3$
286 glasses (Fig. 4a). The difference between Mg-O and Ca-O distances in $MgSiO_3$ and $CaSiO_3$
287 glasses have also been observed in previous ambient pressure study, and is considered to be
288 due to the different ionic radius of M cation (e.g., Cormier and Cuello, 2013). Our results
289 show that the M-O peak positions of $MgSiO_3$ and $CaSiO_3$ glasses show almost no change
290 with varying pressure. Similarly to our results, the experimental results of Salmon et al.
291 (2019) also show almost no change in the M-O distances and coordination numbers at the
292 pressure conditions below ~5 GPa, although Salmon et al. (2019) shows increase of M-O
293 coordination number in $MgSiO_3$ and $CaSiO_3$ glasses at higher pressures than 6 GPa. These
294 data indicate that nearest neighbor Si-O and M-O distances do not change at the pressure
295 conditions of this study up to 5.4 GPa.

296 The intermediate range Si-Si distance of $MgSiO_3$ glass markedly decreases with
297 increasing pressure (Fig. 4b), and it causes shrinking of Si-O-Si angle ($\theta = 2 \cdot$
298 $arcsin[(|Si - Si|/2)/|Si - O|]$) at high pressures (Fig. 5). It has been known that high-
299 pressure structural change of SiO_2 glass occurs mainly by decreasing Si-O-Si angle at high

pressures (e.g., Sonneville et al., 2013). Similarly to SiO_2 glass, Ryu et al. (2022) has also reported decrease of Si-O-Si angle in $MgSiO_3$ glass with increasing pressure. We therefore consider that the pressure-induced structural change in $MgSiO_3$ glass up to 5.2 GPa is attributed to the decrease of Si-O-Si angle, as same as well-known compression behavior in SiO_2 glass (e.g., Sonneville et al., 2013). On the other hand, $CaSiO_3$ glass shows almost no change in the r_4 peak position with varying pressure (Fig. 4), which indicate both Si-Si and Ca-Si distances at ~3.0 Å do not change at high pressures. The calculated Si-O-Si and Ca-O-Si angles of the $CaSiO_3$ glass show almost no change with increasing pressure (Fig. 5), which is different from the marked decrease of the Si-O-Si angle in $MgSiO_3$ glass at high pressures. In exchange for the almost no change in Si-O-Si and Ca-Si-O angles, the $g(r)$ of $CaSiO_3$ glass at high pressures show marked increase of the r_4 peak intensity accompanied with the decrease of the r_5 peak intensity (Fig. 2d). Although the r_5 (Ca-Si/Ca-Ca) peak position of $CaSiO_3$ glass slightly shortens with increasing pressure (0.8 % between ambient and 5.4 GPa) (Fig. 4b), it is not as large as the shortening of the Si-Si peak position in $MgSiO_3$ glass at high pressures (1.8 % between ambient and 5.2 GPa).

These data indicate marked difference in the high-pressure behavior of intermediate range structures of $MgSiO_3$ and $CaSiO_3$ glasses. There are two important

317 structural parameters to discuss intermediate range structure in silicate glasses. One is Q^n
318 species, which represents the number of bridging oxygens (n) connected with a tetrahedral
319 cation (e.g., Mysen, 1990; Stebbins et al., 1992). Salmon et al. (2019) has shown pressure
320 dependence of Q^n species in $MgSiO_3$ and $CaSiO_3$ glasses calculated by MD simulations.
321 The MD simulations of Salmon et al. (2019) show that both $MgSiO_3$ and $CaSiO_3$ glasses
322 consist of ~50% of Q^2 species with ~25% of Q^1 and Q^3 species, which are consistent with
323 those reported by ^{29}Si NMR measurements at ambient pressure for $MgSiO_3$ (Sen et al.
324 2009; Davis et al., 2011) and $CaSiO_3$ (Zhang et al., 1997; Kaseman et al., 2015) glasses.
325 The fractions of the Q^n species in both $MgSiO_3$ and $CaSiO_3$ glasses show only little change
326 with varying pressure at least below 10 GPa (Salmon et al., 2019). The data indicate that Q^n
327 species do not change in both $MgSiO_3$ and $CaSiO_3$ glasses at least in the pressure
328 conditions of this study up to 5.4 GPa. We therefore consider that Q^n species are not
329 structural origin of our obtained different high-pressure behavior in the intermediate range
330 structures of $MgSiO_3$ and $CaSiO_3$ glasses (Figs. 4 and 5).

331 Another important structural parameter to discuss pressure-induced structural change
332 in silicate glasses is polyhedron connectivity (e.g., Lan et al., 2017; Hasmy et al. 2021). It
333 has been reported in theoretical studies that SiO_x polyhedrons of silicate glasses connect by

corner-shared, edge-shared, and/or face-shared configurations, and the polyhedron connectivity may change with varying pressure (e.g., Lan et al., 2017; Hasmy et al. 2021). A molecular dynamics simulation study showed that $CaSiO_3$ glass has similar polyhedron connectivity structure to wollastonite (Mead and Mountjoy, 2006b). We therefore consider polyhedron connectivity in $CaSiO_3$ glass based on the wollastonite structure as a structural motif. In wollastonite, SiO_4 tetrahedra and CaO_6 octahedra forms corner-shared SiO_4-SiO_4 and edge-shared CaO_6-CaO_6 structures. These configurations yield the average Si-Si distance of 3.14±0.04 Å and the average Ca-Ca distance of 3.58±0.11 Å, respectively (Ohashi, 1984). On the other hand, there are two Ca-Si distances in wollastonite crystal structure formed by the corner-shared (3.65±0.16 Å) and edge-shared (3.10±0.03 Å) configurations of SiO_4 tetrahedron and CaO_6 octahedron (Ohashi, 1984). The two Ca-Si distances of the corner-shared and edge-shared CaO_6-SiO_4 configurations in the $CaSiO_3$ structural motif correspond to the r_5 and r_4 peak positions, respectively, in $CaSiO_3$ glass in this study. Then, our data imply that the change of the peak intensity between the r_4 and r_5 peaks obtained in the $g(r)$ of $CaSiO_3$ glass at high pressures (Fig. 2d) can be due to the structural change in the CaO_6-SiO_4 configuration. At low pressures up to 0.8 GPa, low r_4 peak intensity implies that the r_4 peak is mainly composed of the SiO_4-SiO_4 structure and

that the fraction of the edge-shared CaO_6-SiO_4 structure is low. The low contribution of the edge-shared CaO_6-SiO_4 structure on the r_4 peak is consistent with previous molecular dynamics simulation study of $CaSiO_3$ glass at ambient pressure (Mead and Mountjoy, 2006b). On the other hand, at high pressures, the intensity of the r_4 peak markedly increases accompanied with decreasing intensity of the r_5 peak (Fig. 2d). From the previous simulation study of SiO_2 glass (Hasmy et al., 2021), Si-Si coordination number does not change at the pressure conditions below 5.4 GPa. Furthermore, the Raman spectroscopy observations of $CaSiO_3$ glass below 5 GPa (Kubicki et al., 1992; Wolf and McMillan, 1995) show no change in the vibrational spectra related to SiO_4 polyhedral units with increasing pressure at least below 5 GPa, although it starts to change above 10 GPa. Therefore, we interpret the r_4 peak intensity change as the increase of the fraction of the edge-shared CaO_6-SiO_4 structure accompanied with decrease of the fraction of the corner-shared CaO_6-SiO_4 structure (the decrease of the intensity of the r_5 peak) at high pressures. The interpretation of the high-pressure structural behavior of $CaSiO_3$ glass at the pressure conditions less than 5.4 GPa is consistent with previous molecular dynamics simulations (e.g., Mead and Mountjoy, 2006a; Shimoda and Okuno, 2006). Mead and Mountjoy (2006a) investigated pressure-induced structural change in $CaSiO_3$ glasses at 0, 5, and 10

368 GPa, and showed that the intensity of the Ca-Si peak at ~ 3.1 Å increases with increasing
369 pressure. In addition, Shimoda and Okuno (2006) also showed increase of the Ca-Si peak at
370 ~3.1 Å accompanied with decrease of the Ca-Si peak ~3.6 Å between 0 and 7.5 GPa. Thus,
371 our data suggest that compression of $CaSiO_3$ glass at high pressures up to 5.4 GPa occurs
372 through the modification of the CaO_6-SiO_4 structure from the corner-shared configuration
373 to the edge-shared configuration without changing the SiO_4-SiO_4 structure.
374

375 **Implications**

376 In this study, we observed different structural behavior in $CaSiO_3$ and $MgSiO_3$ glasses
377 at high pressures. The different high-pressure structural behavior is also likely present in
378 $CaSiO_3$ and $MgSiO_3$ melts, as Funamori et al. (2004) reported different behavior in the
379 FSDP position at high pressures as same as our observations (Fig. 3). $MgSiO_3$ glass shows
380 marked shift of the position of the FSDP with increasing pressure, while $CaSiO_3$ glass
381 shows only small change in the FSDP position at high pressures (Fig. 3). The different
382 behavior of the FSDP position in $MgSiO_3$ and $CaSiO_3$ glasses obtained in this study are
383 similar to those in $MgSiO_3$ and $CaSiO_3$ melts reported in Funamori et al. (2004) (Fig. 3).
384 These data imply possible presence of intrinsic high-pressure structural difference due to

385 different cation of Mg and Ca in both silicate glass and melt, and its importance in
386 understanding nature and properties of silicate magmas in the Earth's upper mantle. For
387 example, it has been known that viscosity of supercooled liquid $MgSiO_3$-$CaSiO_3$
388 compositions show deep minima in the viscosity-composition relationship (Neuville and
389 Richet, 1991), which is difficult to be interpreted by common viscosity-NBO/T (non-
390 bridging oxygen (NBO) per tetrahedrally coordinated cation (T)) model (e.g., Bottinga and
391 Weil, 1972; Shaw, 1972; Giordano and Dingwell, 2003). In addition, Cochain et al. (2017)
392 reported different high-pressure behavior in the viscosity of $MgSiO_3$ and $CaSiO_3$ melts.
393 $CaSiO_3$ melt (103.6 mPa s at 6.4 GPa and 2128 K) has markedly higher viscosity than
394 $MgSiO_3$ melt (53.5 mPa s at 6.3 GPa and 2148 K) at high pressures. Furthermore,
395 molecular dynamics simulations by Zhang et al. (2010) showed that the difference in
396 viscosity between $CaSiO_3$ and $MgSiO_3$ melts becomes larger at 20 GPa. Our observed
397 different high-pressure structural behavior between $CaSiO_3$ and $MgSiO_3$ glasses may be
398 structural origin of the marked difference in the viscosity of $CaSiO_3$ and $MgSiO_3$ melts at
399 high pressures.
400

401 **Author Contributions**

402 N.M.K and Y.K. devised the project, and wrote the manuscript. N.M.K. carried out
403 the experiments with support from Y.K., I.O. and R.H. for the experiment at the beamline
404 16-BM-B in APS, and Y.K., K.O., K.N., and O.S. for the experiment at the beamline
405 BL04B2 and BL37XU in SPring-8. All authors discussed the results on the manuscript.
406

407 **Acknowledgments**

408 This research is supported by JSPS KAKENHI (Grant Numbers: 19KK0093, 20H00201,
409 and 20K22369), JSPS Bilateral Program (Grant Number: JPJSBP120209926), and the
410 SACLA/SPring-8 Basic Development Program. The experiments were conducted at the
411 beamline BL04B2 and BL37XU in SPring-8 (JASRI Proposal No.: 2019B1495,
412 2021A1087 and 2021A1096 for BL04B2 beamline, 2019B1111, 2020A0600, and
413 2021A1068 for BL37XU beamline) and at the beamline 16-BM-B in APS. Portions of this
414 work were performed at HPCAT (Sector 16), Advanced Photon Source (APS), Argonne
415 National Laboratory. HPCAT operations are supported by DOE-NNSA's Office of
416 Experimental Sciences. The Advanced Photon Source is a U.S. Department of Energy
417 (DOE) Office of Science User Facility operated for the DOE Office of Science by Argonne

National Laboratory under Contract No. DE-AC02-06CH11357.

References

Andrault, D., Morard, G., Garbarino, G., Mezouar, M., Bouhifd, M. A., and Kawamoto, T. (2020). Melting behavior of SiO2 up to 120 GPa. Physics and Chemistry of Minerals, 47(2), 1-9.

Bajgain, S., Ghosh, D.B., and Karki, B.B. (2015). Structure and density of basaltic melts; at mantle conditions from first-principles simulations. Nature communications, 6(1), 8578.

Benmore, C.J., Soignard, E., Amin, S.A., Guthrie, M., Shastri, S.D., Lee, P.L., and Yarger, J.L. (2010). Structural and topological changes in silica glass at pressure. Physical Review B, 81(5), 054105.

Bottinga, Y., and Weill, D.F. (1972). The viscosity of magmatic silicate liquids; a model calculation. American journal of science, 272(5), 438-475.

Cochain, B., Sanloup, C., Leroy, C., and Kono, Y. (2017). Viscosity of mafic magmas at high pressures. Geophysical Research Letters, 44(2), 818-826.

Cormier, L., and Cuello, G.J. (2011). Mg coordination in a $MgSiO_3$ glass using neutron diffraction coupled with isotopic substitution. Physical Review B, 83(22), 224204.

Cormier, L., and Cuello, G.J. (2013). Structural investigation of glasses along the $MgSiO_3$–$CaSiO_3$ join: Diffraction studies. Geochimica et Cosmochimica Acta, 122, 498-510.

Davis, M.C., Sanders, K.J., Grandinetti, P.J., Gaudio, S.J., and Sen, S. (2011). Structural Investigations of magnesium silicate glasses by 29Si 2D magic-angle flipping NMR. Journal of Non Crystalline Solids, 357(15), 2787-2795.

De Grouchy, C.J., Sanloup, C., Cochain, B., Drewitt, J.W., Kono, Y., & Crépisson, C. (2017). Lutetium incorporation in magmas at depth: Changes in melt local environment and the influence on partitioning behaviour. Earth and Planetary Science Letters, 464, 155-165.

Faber, T.E., and Ziman, J.M. (1965). A theory of the electrical properties of liquid metals: III. The resistivity of binary alloys. Philosophical Magazine, 11(109), 153-173.

Funamori, N., Yamamoto, S., Yagi, T., and Kikegawa, T. (2004). Exploratory studies of

451 silicate melt structure at high pressures and temperatures by in situ X-ray
452 diffraction. Journal of Geophysical Research: Solid Earth, 109(B3).
453 Giordano, D., and Dingwell, D.B. (2003). Non-Arrhenian multicomponent melt viscosity:
454 a model. Earth and Planetary Science Letters, 208(3-4), 337-349.
455 Ghosh, D.B., Karki, B.B., and Stixrude, L. (2014). First-principles molecular dynamics
456 simulations of $MgSiO_3$ glass: Structure, density, and elasticity at high
457 pressure. American Mineralogist, 99(7), 1304-1314.
458 Hasmy, A., Ispas, S., and Hehlen, B. (2021). Percolation transitions in compressed SiO2
459 glasses. Nature, 599(7883), 62-66.
460 Hosemann, R., and Bagchi, S.N. (1962). Direct analysis of diffraction by matter. North-
461 Holland Publishing Company.
462 Kalampounias, A.G., Nasikas, N.K., and Papatheodorou, G.N. (2009). Glass formation
463 and structure in the $MgSiO_3$–Mg_2SiO_4 pseudobinary system: From degraded
464 networks to ioniclike glasses. The Journal of chemical physics, 131(11), 114513.
465 Kaseman, D.C., Retsinas, A., Kalampounias, A.G., Papatheodorou, G. N., and Sen, S.
466 (2015). Q-speciation and network structure evolution in invert calcium silicate
467 glasses. The Journal of Physical Chemistry B, 119(26), 8440-8445.

468 Kohara, S., Itou, M., Suzuya, K., Inamura, Y., Sakurai, Y., Ohishi, Y., & Takata, M. (2007).
469 Structural studies of disordered materials using high-energy x-ray diffraction from
470 ambient to extreme conditions. Journal of Physics: Condensed Matter, 19(50),
471 506101.
472 Kohara, S., Akola, J., Morita, H., Suzuya, K., Weber, J.K.R., Wilding, M.C., and Benmore,
473 C.J. (2011). Relationship between topological order and glass forming ability in
474 densely packed enstatite and forsterite composition glasses. Proceedings of the
475 National Academy of Sciences, 108(36), 14780-14785.
476 Kono, Y., Irifune, T., Higo, Y., Inoue, T., and Barnhoorn, A. (2010). P–V–T relation of
477 MgO derived by simultaneous elastic wave velocity and in situ X-ray
478 measurements: A new pressure scale for the mantle transition region. Physics of
479 the Earth and Planetary Interiors, 183(1-2), 196-211.
480 Kono, Y., Park, C., Kenney-Benson, C., Shen, G., and Wang, Y. (2014). Toward
481 comprehensive studies of liquids at high pressures and high temperatures:
482 Combined structure, elastic wave velocity, and viscosity measurements in the
483 Paris–Edinburgh cell. Physics of the Earth and Planetary Interiors, 228, 269-
484 280.

485 Kono, Y., Shibazaki, Y., Kenney-Benson, C., Wang, Y., and Shen, G. (2018). Pressure-
486 induced structural change in $MgSiO_3$ glass at pressures near the Earth's core–
487 mantle boundary. Proceedings of the National Academy of Sciences, 115(8),
488 1742-1747.
489 Kono, Y., Shu, Y., Kenney-Benson, C., Wang, Y., and Shen, G. (2020). Structural evolution
490 of SiO_2 glass with Si coordination number greater than 6. Physical Review
491 Letters, 125(20), 205701.
492 Kono, Y., Ohara, K., Kondo, N.M., Yamada, H., Hiroi, S., Noritake, F., ... & Yabashi, M.
493 (2022). Experimental evidence of tetrahedral symmetry breaking in SiO2 glass
494 under pressure. Nature communications, 13(1), 1-8.
495 Kubicki, J.D., Hemley, R.J., and Hofmeister, A.M. (1992). Raman and infrared study of
496 pressure-induced structural changes in MgSiO3, CaMgSi2O6, and CaSiO3
497 glasses. American Mineralogist, 77(3-4), 258-269.
498 Lan, M.T., Duong, T.T., Iitaka, T., and Van Hong, N. (2017). Computer simulation of
499 CaSiO3 glass under compression: Correlation between Si–Si pair radial distribution
500 function and intermediate range order structure. Materials Research Express, 4(6),
501 065201.

Lee, S.K., Lin, J.F., Cai, Y.Q., Hiraoka, N., Eng, P.J., Okuchi, T., ... and Yoo, C.S. (2008). X-ray Raman scattering study of $MgSiO_3$ glass at high pressure: Implication for triclustered $MgSiO_3$ melt in Earth's mantle. Proceedings of the National Academy of Sciences, 105(23), 7925-7929.

Lee, S.K., Kim, Y.H., Yi, Y.S., Chow, P., Xiao, Y., Ji, C., and Shen, G. (2019). Oxygen quadclusters in SiO_2 glass above megabar pressures up to 160 GPa revealed by X-ray Raman scattering. Physical Review Letters, 123(23), 235701.

Lorch, E. (1969). Neutron diffraction by germania, silica and radiation-damaged silica glasses. Journal of Physics C: Solid State Physics, 2(2), 229.

Mead, R.N., and Mountjoy, G. (2006a). A molecular dynamics study of densification mechanisms in calcium silicate glasses Ca Si 2 O 5 and Ca Si O 3 at pressures of 5 and 10 GPa. The Journal of chemical physics, *125*(15), 154501.

Mead, R.N., and Mountjoy, G. (2006b). A molecular dynamics study of the atomic structure of (CaO) x (SiO2) 1-x glasses. The Journal of Physical Chemistry B, 110(29), 14273-14278.

Murakami, M., and Bass, J.D. (2010). Spectroscopic evidence for ultrahigh-pressure polymorphism in SiO_2 glass. Physical Review Letters, 104(2), 025504.

519 Mysen, B.O. (1990). Effect of pressure, temperature, and bulk composition on the structure
520 and species distribution in depolymerized alkali aluminosilicate melts and quenched
521 melts. Journal of Geophysical Research: Solid Earth, 95(B10), 15733-15744.
522 Neuville, D. R., and Richet, P. (1991). Viscosity and mixing in molten (Ca, Mg) pyroxenes
523 and garnets. Geochimica et Cosmochimica Acta, 55(4), 1011-1019.
524 Ohara, K., Onodera, Y., Kohara, S., Koyama, C., Masuno, A., Mizuno, A., ... and Sakata,
525 O. (2020). Accurate synchrotron hard X-ray diffraction measurements on high-
526 temperature liquid oxides. International Journal of Microgravity Science and
527 Application, 37(2), 370202.
528 Ohashi, Y. (1984). Polysynthetically-twinned structures of enstatite and
529 wollastonite. Physics and Chemistry of Minerals, 10(5), 217-229.
530 Petitgirard, S., Sahle, C.J., Weis, C., Gilmore, K., Spiekermann, G., Tse, J.S., ... and
531 Sternemann, C. (2019). Magma properties at deep Earth's conditions from
532 electronic structure of silica. Geochemcal Perspective Letters, 9, 32-37.
533 Prescher, C., Prakapenka, V.B., Stefanski, J., Jahn, S., Skinner, L.B., and Wang, Y. (2017).
534 Beyond sixfold coordinated Si in SiO_2 glass at ultrahigh pressures. Proceedings
535 of the National Academy of Sciences, 114(38), 10041-10046.

536 Ryu, Y.J., Wang, Y., Yu, T., Bonnet, F., Greenberg, E., Prescher, C., … and Rivers, M.L.
537 (2022). A multi-faceted experimental study on the dynamic behavior of $MgSiO_3$
538 glass in the Earth's deep interior. American Mineralogist, 107(7), 1313-1324.
539 Sakamaki, T., Suzuki, A., Ohtani, E., Terasaki, H., Urakawa, S., Katayama, Y., ... and
540 Ballmer, M.D. (2013). Ponded melt at the boundary between the lithosphere and
541 asthenosphere. Nature Geoscience, 6(12), 1041-1044.
542 Salmon, P.S., Moody, G.S., Ishii, Y., Pizzey, K.J., Polidori, A., Salanne, M., ... and
543 MacLeod, S.G. (2019). Pressure induced structural transformations in amorphous
544 $MgSiO_3$ and $CaSiO_3$. Journal of Non-Crystalline Solids: X, 3, 100024
545 Sanloup, C., Drewitt, J.W., Konôpková, Z., Dalladay-Simpson, P., Morton, D.M., Rai,
546 N., ... and Morgenroth, W. (2013). Structural change in molten basalt at deep
547 mantle conditions. Nature, 503(7474), 104-107.
548 Sato, T., and Funamori, N. (2008). Sixfold-coordinated amorphous polymorph of SiO_2
549 under high pressure. Physical review letters, 101(25), 255502.
550 Sen, S., Maekawa, H., and Papatheodorou, G.N. (2009). Short-range structure of invert
551 glasses along the pseudo-binary join MgSiO3− Mg2SiO4: Results from 29Si and
552 25Mg MAS NMR spectroscopy. The Journal of Physical Chemistry B, 113(46),

553 15243-15248.

554 Shaw, H.R. (1972). Viscosities of magmatic silicate liquids; an empirical method of
555 prediction. American Journal of Science, 272(9), 870-893.

556 Shimoda, K., Miyamoto, H., Kikuchi, M., Kusaba, K., and Okuno, M. (2005). Structural
557 evolutions of CaSiO3 and CaMgSi2O6 metasilicate glasses by static
558 compression. Chemical Geology, 222(1-2), 83-93.

559 Shimoda, K., and Okuno, M. (2006). Molecular dynamics study of CaSiO3–MgSiO3
560 glasses under high pressure. Journal of Physics: Condensed Matter, 18(28), 6531.

561 Sonneville, C., Deschamps, T., Martinet, C., de Ligny, D., Mermet, A., and Champagnon,
562 B. (2013). Polyamorphic transitions in silica glass. Journal of non-crystalline
563 solids, 382, 133-136.

564 Stebbins, J.F., Farnan, I., and Xue, X. (1992). The structure and dynamics of alkali silicate
565 liquids: A view from NMR spectroscopy. Chemical Geology, 96(3-4), 371-385.

566 Tsuchiya, T. (2003). First-principles prediction of the P-V-T equation of state of gold and
567 the 660-km discontinuity in Earth's mantle. Journal of Geophysical Research:
568 Solid Earth, 108(B10).

569 Wang, Y., Sakamaki, T., Skinner, L.B., Jing, Z., Yu, T., Kono, Y., ... and Sutton, S. R.

(2014). Atomistic insight into viscosity and density of silicate melts under pressure. Nature communications, 5(1), 3241.

Wolf, G.H., and McMillan, P.F. (1995). Pressure effects on silicate melt structure and properties. Reviews in Mineralogy and Geochemistry, 32(1), 505-561.

Zhang, P., Grandinetti, P.J., and Stebbins, J.F. (1997). Anionic species determination in CaSiO3 glass using two-dimensional 29Si NMR. The Journal of Physical Chemistry B, 101(20), 4004-4008.

Zhang, L., Van Orman, J.A., and Lacks, D.J. (2010). Molecular dynamics investigation of $MgO–CaO–SiO_2$ liquids: Influence of pressure and composition on density and transport properties. Chemical Geology, 275(1-2), 50-57.

List of figure captions

Figure 1. Structure factor, $S(Q)$, and pair distribution function, $g(r)$, of $MgSiO_3$ glass (**a, b**) and of $CaSiO_3$ glass (**c, d**) at ambient pressure. (**b**) r_1, r_2, r_3, and r_4 are Si-O, Mg-O, O-O, and Si-Si/Mg-Si/Mg-Mg distances, respectively. (**d**) r_1, r_2, r_3, r_4 and r_5 are Si-O, Ca-O, O-O, Si-Si, and Ca-Si/Ca-Ca distances, respectively.

587

588 **Figure 2.** Structure factor, $S(Q)$, and pair distribution function, $g(r)$, of $MgSiO_3$ glass (**a, b**)
589 and $CaSiO_3$ glass (**c, d**) at high pressures. (**b**) r_1, r_2, and r_4 are Si-O, Mg-O, and Si-Si/Mg-
590 Si/Mg-Mg distances, respectively. (**d**) r_1, r_2, r_4 and r_5 are Si-O, Ca-O, Si-Si, and Ca-Si/Ca-
591 Ca distances, respectively.

592

593 **Figure 3.** Position of the first sharp diffraction peak (FSDP) in $S(Q)$ of $CaSiO_3$ and $MgSiO_3$
594 glasses at high pressures, compared with those of $CaSiO_3$ and $MgSiO_3$ melts reported in
595 Funamori et al. (2004). Solid red squares and solid black triangles represent the FSDP
596 positions of $CaSiO_3$ and $MgSiO_3$ glasses, respectively, obtained in this study. Sizes of the
597 errors in $CaSiO_3$ glass results are smaller than the size of the symbol. Open red squares and
598 open black triangles represent the FSDP positions of $CaSiO_3$ and $MgSiO_3$ melts,
599 respectively, reported in Funamori et al. (2004). Vertical bars on the symbols represent the
600 size of the error. Several data have the error bar smaller than the symbol size.

601

602

603 **Figure 4.** Peak positions in $g(r)$ of $CaSiO_3$ and $MgSiO_3$ glasses form ambient to around 5

GPa. Red solid squares and black solid triangles represent peak positions of $CaSiO_3$ and $MgSiO_3$ glasses, respectively. Vertical bars on the symbols represent the size of the error. Several data have the error bar smaller than the symbol size.

Figure 5. Si-O-Si angle of $MgSiO_3$ glasses and Si-O-Si/Ca-O-Si angles of $CaSiO_3$ glass as a function of pressure. The Si-O-Si angle (θ) was calculated by using simple sine relation ($\theta = 2 \cdot arcsin[(|Si - Si|/2)/|Si - O|]$). Vertical bars on the symbols represent the size of the error. Several data have the error bar smaller than the symbol size.

Table 1. Positions of the first sharp diffraction peak (FSDP) of *S*(*Q*), peak positions in *g*(*r*), Si-O-Si angle of $MgSiO_3$, and Si-O-Si and Ca-O-Si angles of $CaSiO_3$ glasses at ambient and high pressure conditions.

$MgSiO_3$ glass	Ambient	1.0 GPa	1.9 GPa	3.0 GPa	4.3 GPa	5.2 GPa
FSDP ($Å^{-1}$)	1.88(±0.01)	1.93(±0.01)	1.94(±0.01)	1.96(±0.01)	2.01(±0.05)	2.03(±0.06)
Si-O (Å)	1.621(±0.002)	1.613(±0.002)	1.618(±0.002)	1.616(±0.002)	1.605(±0.003)	1.614(±0.009)
Mg-O (Å)	2.030(±0.004)	2.026(±0.006)	2.004(±0.005)	2.050(±0.004)	2.027(±0.007)	2.055(±0.004)
O-O (Å)	2.65(fixed)	2.65(fixed)	2.65(fixed)	2.65(fixed)	2.65(fixed)	2.65(fixed)
Si-Si (Å)	3.179(±0.006)	3.171(±0.002)	3.168(±0.002)	3.134(±0.013)	3.113(±0.003)	3.122(±0.011)
Mg-Si (Å)	3.220(±0.006)	3.226(±0.006)	3.234(±0.008)	3.210(±0.006)	3.206(±0.007)	3.209(±0.004)
Mg-Mg	3.42(fixed)	3.42(fixed)	3.42(fixed)	3.42(fixed)	3.42(fixed)	3.42(fixed)
Si-O-Si angle (°)	137.3(±0.8)	135.8(±0.5)	133.9(±0.6)	133.8(±0.6)	133.7(±0.9)	130.9(±1.4)

$CaSiO_3$ glass	Ambient	0.8 GPa	2.3 GPa	3.3 GPa	4.6 GPa	5.4 GPa
FSDP ($Å^{-1}$)	2.137(±0.005)	2.154(±0.003)	2.168(±0.001)	2.177(±0.002)	2.189(±0.003)	2.200(±0.002)
Si-O (Å)	1.622(±0.001)	1.618(±0.003)	1.616(±0.003)	1.621(±0.003)	1.611(±0.003)	1.614(±0.003)
Ca-O (Å)	2.302(±0.001)	2.315(±0.004)	2.306(±0.004)	2.305(±0.004)	2.298(±0.004)	2.297(±0.004)
O-O (Å)	2.611(±0.007)	2.611(fixed)	2.611(fixed)	2.611(fixed)	2.611(fixed)	2.611(fixed)
Si-Si, Ca-Si (Å)	3.017(±0.008)	2.997(±0.026)	2.998(±0.032)	2.998(±0.014)	2.998(±0.018)	2.996(±0.001)
Ca-Si, Ca-Ca (Å)	3.573(±0.014)	3.569(±0.015)	3.550(±0.021)	3.557(±0.026)	3.554(±0.013)	3.554(±0.015)
Si-O-Si and Ca-O-Si angles (°)	136.8(±0.8)	135.6(±2.5)	136.2(±3.0)	135.4(±1.4)	137.0(±1.8)	136.3(±1.2)

616

This is the peer-reviewed, final accepted version for American Mineralogist, published by the Mineralogical Society of America.
The published version is subject to change. Cite as Authors (Year) Title. American Mineralogist, in press.
DOI: https://doi.org/10.2138/am-2023-9060. http://www.minsocam.org/

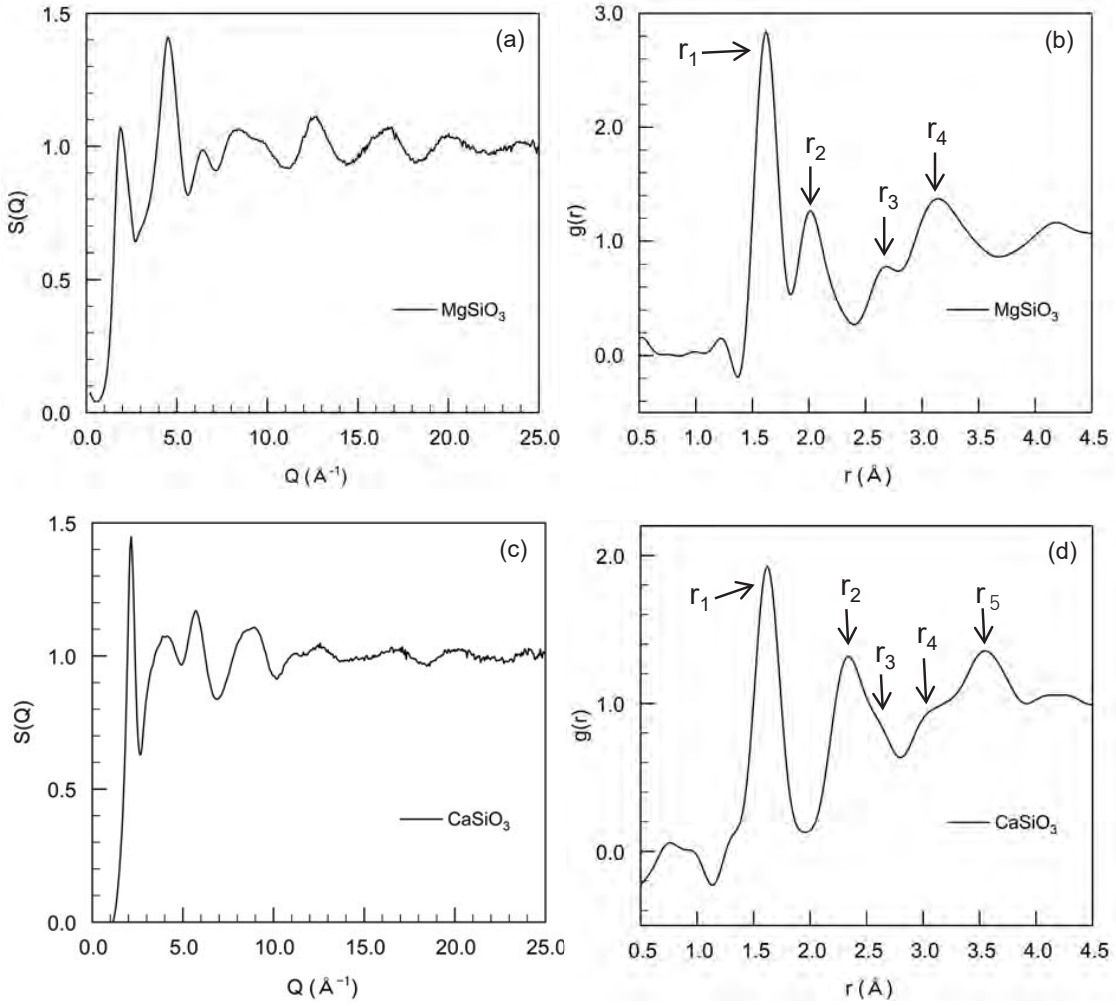

Figure 1

This is the peer-reviewed, final accepted version for American Mineralogist, published by the Mineralogical Society of America.
The published version is subject to change. Cite as Authors (Year) Title. American Mineralogist, in press.
DOI: https://doi.org/10.2138/am-2023-9060. http://www.minsocam.org/

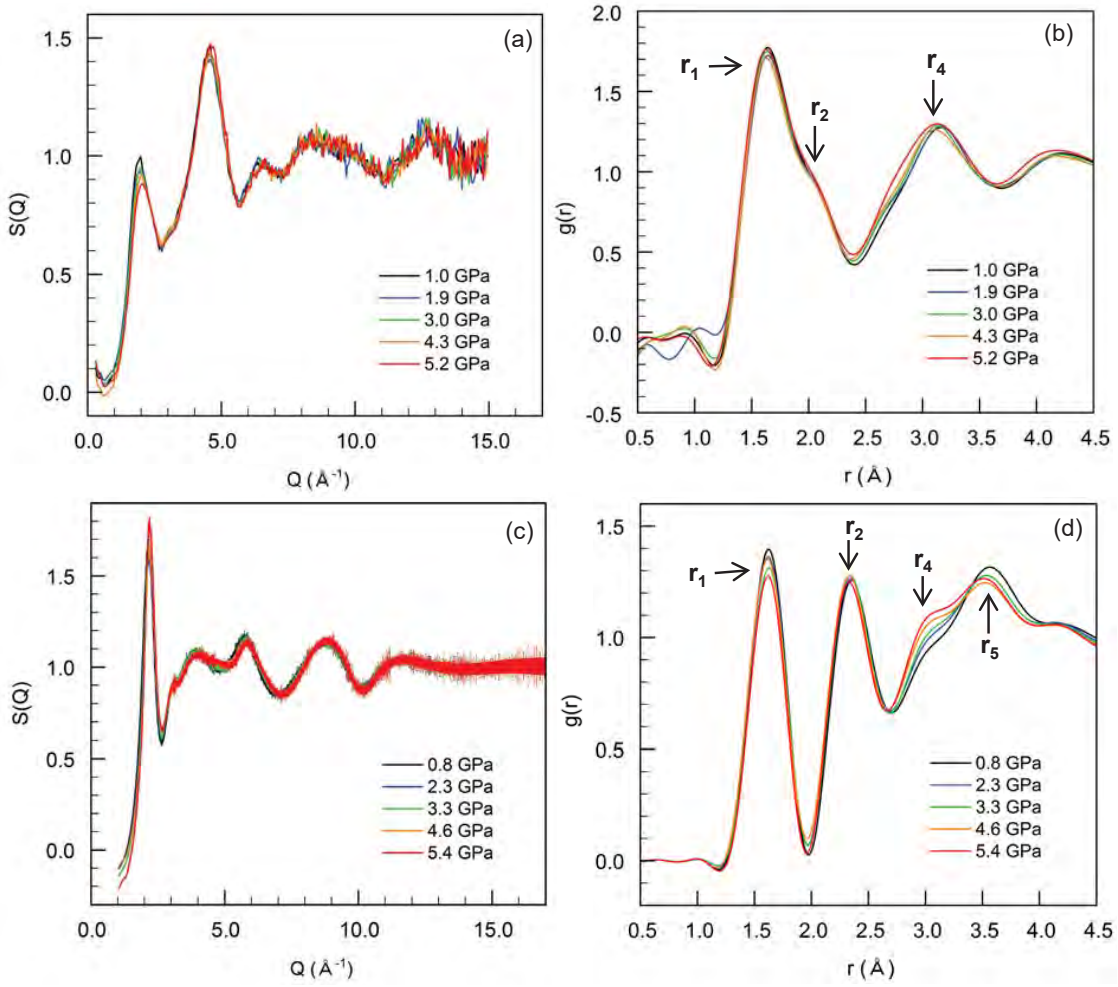

Figure 2

This is the peer-reviewed, final accepted version for American Mineralogist, published by the Mineralogical Society of America.
The published version is subject to change. Cite as Authors (Year) Title. American Mineralogist, in press.
DOI: https://doi.org/10.2138/am-2023-9060. http://www.minsocam.org/

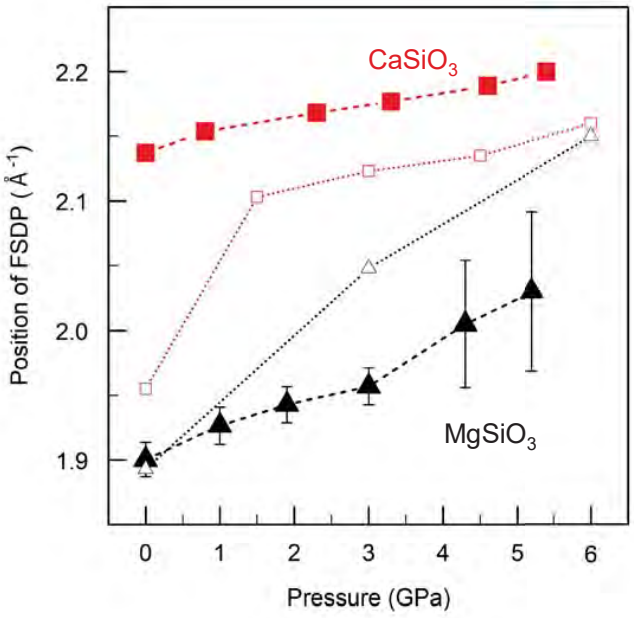

Figure 3

This is the peer-reviewed, final accepted version for American Mineralogist, published by the Mineralogical Society of America.
The published version is subject to change. Cite as Authors (Year) Title. American Mineralogist, in press.
DOI: https://doi.org/10.2138/am-2023-9060. http://www.minsocam.org/

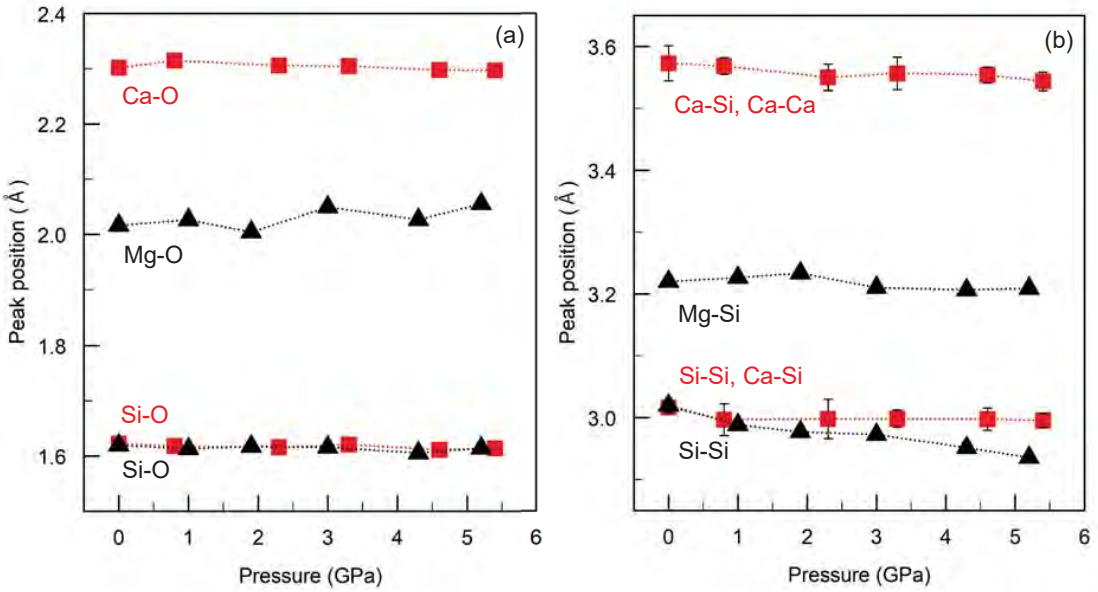

Figure 4

This is the peer-reviewed, final accepted version for American Mineralogist, published by the Mineralogical Society of America.
The published version is subject to change. Cite as Authors (Year) Title. American Mineralogist, in press.
DOI: https://doi.org/10.2138/am-2023-9060. http://www.minsocam.org/

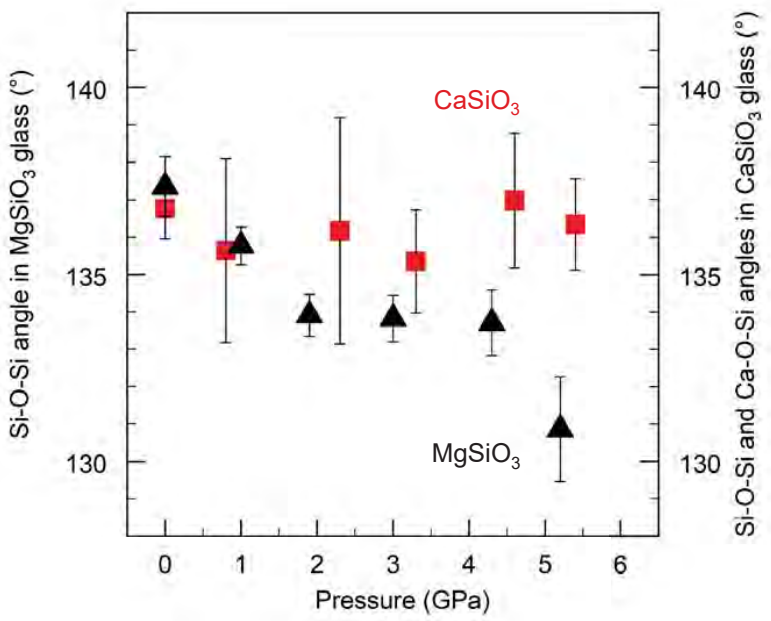

Figure 5